J. Linnemann, J. Giorgio, K. Wagner, G. Mathieson, G. G. Wallace, D. L. Officer

A simple one step process for enhancement of titanium foil dye sensitised solar cell anodes

Erstveröffentlichung in / First published in:
Journal of Materials Chemistry A. 2015, 3(7), S. 3266–3270 [Zugriff am: 01.11.2019]. Royal Society of Chemistry. ISSN 2050-7496.

DOI: https://doi.org/10.1039/c4ta05407e

Journal of Materials Chemistry A

COMMUNICATION

View Article Online
View Journal | View Issue

Cite this: J. Mater. Chem. A, 2015, 3, 3266

Received 10th October 2014
Accepted 7th January 2015

DOI: 10.1039/c4ta05407e

www.rsc.org/MaterialsA

A simple one step process for enhancement of titanium foil dye sensitised solar cell anodes†

J. Linnemann,[bc] J. Giorgio,[a] K. Wagner,[a] G. Mathieson,[a] G. G. Wallace[a] and D. L. Officer*[a]

The photo-conversion efficiency and stability of back-illuminated dye sensitised solar cells with titanium foil based photoanodes are enhanced by a simple nitric acid treatment through which the foil is passivated. This treatment changes the morphology of the titanium foil and increases its electrochemical double layer capacitance.

Dye sensitised solar cells (DSSCs) are of high interest in research and for industrial applications due to the low-cost materials needed for their fabrication and their excellent performance in a broader range of light conditions compared to silicon solar cells. A solar cell design working under back-illumination offers the possibility of employing a thin metal foil as substrate of the photoanode giving the advantage of flexibility and much lower sheet resistance than a transparent conductive oxide glass based electrode. Titanium-based photoanodes show less surface state trapping and suppression of the back reaction of electrons with triiodide ions of the electrolyte because of a natural titanium dioxide (TiO_2) passivation layer.[1] Furthermore, the incident photon-to-current conversion efficiency (IPCE) of DSSCs with titanium (Ti) foil anode substrates is higher in the red-region due to the light reflection properties of Ti.[2]

The performance of DSSCs with Ti foil as photoanode substrate has been further improved by introducing TiO_2 interlayers between the anode substrate and the absorbing mesoscopic TiO_2 film. This has been typically achieved by chemical treatments involving hydrogen peroxide (H_2O_2) with a variety of conditions.[3–8] The enhancement is assigned to improved electrical contact due to a higher electrode surface area, retarding of the recombination reaction, extra-dye-uptake by the interlayer and increased light reflection.

We were interested in taking advantage of these enhancements for the development of flexible DSSCs but were unable to obtain the reported improvements. Therefore, we undertook a more detailed investigation of the chemical treatment of Ti foil as a way to improve the performance of DSSC photoanodes.

In this study, thicker, nanostructured TiO_2 layers were introduced on native as well as passivated Ti foils, and the foil employed as anode substrates in DSSCs. For this, cleaned as-received Ti foils were treated with H_2O_2 under high reaction rate conditions (high temperature, limited period of time) and low reaction rate conditions (room temperature, long period of time) or the same treatments were carried out on Ti foils previously treated with 30% nitric acid (HNO_3), a well-known passivating agent for Ti.[9] Surprisingly, despite an obvious surface area increase with H_2O_2 treatments, the best performance enhancement of the back-illuminated DSSC was achieved using only the simple HNO_3 treatment. No laborious chemical etching or polishing pre-treatments are necessary. The passivation layer is highly resistant to corrosive electrolytes,[6] leading to a longer device lifetime. Further investigations demonstrated that the efficiency increase of the photoanode is mainly due to improved electron transport properties in the mesoscopic TiO_2 film as a result of better electrical contact.

Titanium and its alloys are commonly used as implant materials in medicine and different surface treatments, including passivation of titanium in nitric acid, have been investigated. This kind of treatment has been found to efficiently remove surface contaminations such as transition metals and improve the homogeneity of passivated films at local defect sites.[10] Ti has a *ca.* 2 nm thick natural passivation layer[11] that is already present on the as-received foil.

For cleaning and passivation purposes, the foil was dipped for 24 hours into 30% HNO_3. The scanning electron microscopy (SEM) image (Fig. 1b) shows the changes in the Ti surface morphology due to this passivation treatment. While the native

[a]ARC Centre of Excellence for Electromaterials Science and Intelligent Polymer Research Institute, AIIM Facility, University of Wollongong, Wollongong, NSW 2522, Australia. E-mail: davido@uow.edu.au

[b]Leibniz Institute for Solid State and Materials Research (IFW) Dresden, Helmholtzstraße 20, 01069 Dresden, Germany

[c]Physical Chemistry, TU Dresden, Bergstraße 66b, 01062 Dresden, Germany

† Electronic supplementary information (ESI): Detailed experimental procedures for surface treatments of Ti foil, DSSCs assembling, characterisation measurements, and SEM images of Ti foil after passivation in HNO_3 and then etched in H_2O_2 are available. See DOI: 10.1039/c4ta05407e

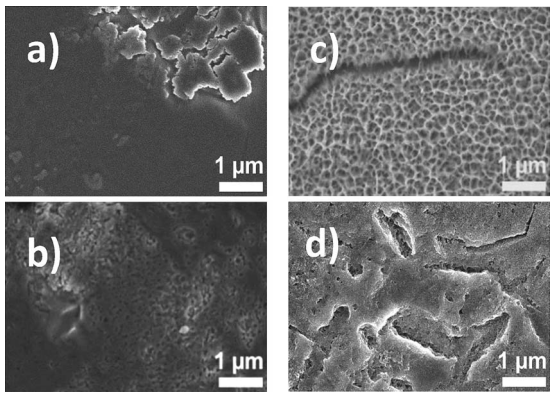

Fig. 1 SEM images of native titanium foil (a), passivated in HNO_3 (b), native foil etched in H_2O_2 for 1 h at 95 °C (c), or native foil etched in H_2O_2 for 48 h at room temperature (d).

foil is smooth with isolated defect sites (Fig. 1a), the HNO_3 treated foil has significantly increased fine grained surface roughness (Fig. 1b). As reported by Sitting *et al.*[10] the overall surface topography of pure titanium surfaces is not affected by nitric acid treatment, therefore the examined commercial Ti foil is not pure. In this study, we successfully employed cross sectional SEM images with ion milling to measure the change in thickness of introduced TiO_2 interlayers (see below and ESI† for details). However, we were unable to do so for this passivation layer as it was too thin to be observed by SEM.

In order to probe the effect of this surface modification, open circuit potential and capacitance measurements were undertaken. As shown in Fig. 2, the open circuit potential of a piece of titanium foil exposed to HNO_3 decreases significantly during the first 10 hours and then stabilizes around 380 mV *vs.* Ag/AgCl, indicative of the surface transformation on the foil (Fig. 1b). The capacitance of the Ti foil was measured using cyclic voltammetry (CV) (insets, Fig. 2). The voltammogram shows a rectangular shape and an immediate current response when changing the scan direction, (Fig. 2) resulting from the electrochemical double layer capacitance of the electrode surface. The capacitance of the passivated Ti foil is 51 μF cm^{-2}, which is higher than the native foil at 34 μF cm^{-2}. Thus the electrochemically active surface area of the TiO_2 layer on the foil increases during the HNO_3 treatment.

Both types of Ti foil, native and passivated, were further treated with H_2O_2 to grow nanostructured titania layers between the Ti foil substrate and the screen-printed TiO_2 working electrode material. The H_2O_2 etching was performed under high reaction rate conditions (95 °C, closed reaction vessel) for short time periods (20 min and 60 min)[7] as well as at room temperature for 48 h,[3] as the reaction rate significantly affects the titania film formation.[12] As shown in Fig. 1c and d, different surface morphologies were obtained. After 1 h in H_2O_2 at 95 °C, a porous sponge-like structure with some micrometre-long cracks is observed on the foil, a structure remarkably similar to that of Wu *et al.*[12] who treated acid passivated foil with 15% H_2O_2 for 1 h at 80 °C, but unlike that of Tsai and co-workers[7] whose conditions we attempted to replicate. The layer thickness was determined to be 1.2 μm using cross sectional SEM images of ion milled samples (for details, see ESI†). While there is no noticeable difference between the passivated (Fig. S1a†) and native (Fig. 1c) foils for this H_2O_2 treatment, the samples that were immersed in a H_2O_2 solution for 48 h at room temperature differ somewhat from each other. The structure on the native foil (Fig. 1d) shows a smooth surface between the defects rather than the very finely etched surface of the passivated samples (Fig. S1b†). The achieved layer thicknesses of about 1.8 μm are larger than for the high reaction rate conditions. The foils etched with hydrogen peroxide at 95 °C for just 20 min were only partly covered with titania layers and led to diminished photovoltaic performance compared to all other foil samples when employed in DSSCs and were not investigated further.

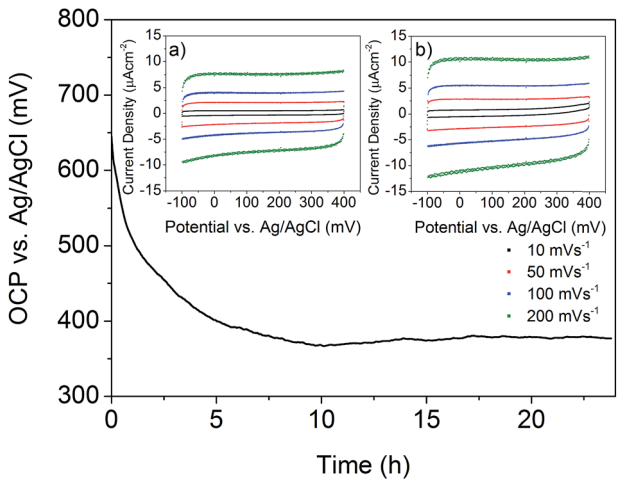

Fig. 2 Open circuit potential–time transient of Ti foil in HNO_3 measured for 24 h. Inserts: cyclic voltammograms in 1 M Na_2SO_4 solution at scan rates ranging from 10 to 200 mV s^{-1} of native Ti foil (a), and in HNO_3 passivated Ti foil (b).

Table 1 Photovoltaic performance of back-illuminated DSSCs with differently treated Ti foils as working electrode substrate under full simulated AM 1.5 illumination. All devices are fabricated with ruthenium dye N719 with an iodine/iodide redox couple. Efficiency error calculations are based on a confidence interval of 95%

Treatment	J_{SC} (mA cm^{-2})	V_{OC} (V)	FF	η (%)
None	8.85	760	0.70	4.8 ± 0.4
After 20 days	*3.04*	*710*	*0.73*	*1.8 ± 0.3*
HNO_3 passivation	9.87	770	0.74	5.6 ± 0.1
After 20 days	*9.08*	*780*	*0.78*	*5.5 ± 0.2*
1 h H_2O_2, 95 °C	6.13	730	0.63	2.8 ± 0.2
HNO_3 and 1 h H_2O_2, 95 °C	9.42	770	0.71	5.1 ± 0.2
After 20 days	*6.65*	*750*	*0.74*	*3.7 ± 0.2*
48 h H_2O_2, RT	3.44	740	0.65	1.6 ± 1.2
HNO_3 and 48 h H_2O_2, RT	10.12	760	0.73	5.6 ± 0.2
After 20 days	*8.4*	*780*	*0.77*	*5.0 ± 0.1*

Table 1 summarises the photovoltaic performances of the back-illuminated DSSCs, which were assembled using the differently treated Ti foils as the working electrode substrate. The energy conversion efficiency (η) increases about 17% for the HNO_3 passivated foil compared to the native foil. This simple HNO_3 passivation treatment results in efficiency of 5.6%, the highest achieved here. The TiO_2 interlayers produced by chemical etching of the native Ti foil in H_2O_2 cause a remarkable drop in the photovoltaic performance of the corresponding DSSCs from 4.8% to 2.8% or rather 1.6%. The solar cells made with Ti foils treated in H_2O_2 after passivation are more efficient than devices where native foils are employed but less or equally efficient than devices using just passivated Ti foils. The efficiency trends between the various substrates are reflected in all of the other photovoltaic parameters (short-circuit current J_{SC}, open circuit potential V_{OC} and fill factor FF). All in all, the HNO_3 treatment appears to be crucial for the enhancement of the solar cell performance and spectroscopic analysis of the foils was carried out to gain a better understanding of the effect of the HNO_3 passivation layer.

Raman spectroscopy measurements were conducted to identify the titania phase of the layers on the foils (Fig. 3). All substrates were thermally annealed (500 °C) prior to measurement to ensure that the TiO_2 layers on the foils were in the same state as obtained in the solar cell, even though during the normal fabrication process annealing was performed after screen printing of the nanoparticle paste. As clearly evident from Fig. 3, the natural layer of the native foil as well as the one present after the HNO_3 passivation treatment are in the rutile phase. The 1.8 μm thick titania layer on the first-passivated Ti foil immersed in H_2O_2 for 48 h also shows only signals that can be assigned to rutile. However, the H_2O_2 treatment performed for 1 h at 95 °C leads to an anatase layer of high crystallinity. The intensity of the Raman peaks is much higher than for the other treatments.

To study the influence of the passivation treatment on the electron transport processes in DSSCs, electrochemical impedance spectroscopy (EIS) was carried out at the open-circuit voltage under illumination of AM 1.5 in a frequency range of 0.3 MHz to 2 Hz. The corresponding Nyquist plots are displayed in Fig. 4. The appearance of multiple semicircles (typically three or four) in the impedance spectrum indicates the existence of a series of electron transfers (with different time constants) occurring at electrochemical interfaces within the investigated devices.[16,17] The lower frequency range is usually attributed to Nernstian diffusion within the electrolyte. In our case, due to the negligibly thin layer of electrolyte (25 μm spacer) and the investigated frequency range, we do not see the impedance related to this diffusion. Three semicircles are observed in Fig. 4 although two of them are overlapping. The main arc is assigned to the electrolyte/dye/TiO_2 interface and is related to the reverse electron transfer from the TiO_2 to the electrolyte. The remaining two overlapping semicircles at higher frequency result from electron transfer processes between the nanoparticles of the mesoscopic TiO_2 film (lower frequency part) and to both the interface between the TiO_2 nanoparticles and the electrode substrate material (Ti), and the counter electrode (higher frequency part).

To interpret impedance data of DSSCs, mostly with glass-based working electrodes, transmission line models have been used consisting of two parallel channels that are connected *via* charge-transfer processes on the TiO_2/electrolyte interface, as well as simplified forms.[18–20] The resistances obtained with the equivalent circuit in Fig. 4 (inset) are given in Table 2. R_S is the series resistance, which is mainly related to the sheet resistance of the electrode substrates and contact resistances of the electrical circuit. The capacitance of the mesoscopic TiO_2 film C_{TiO_2}

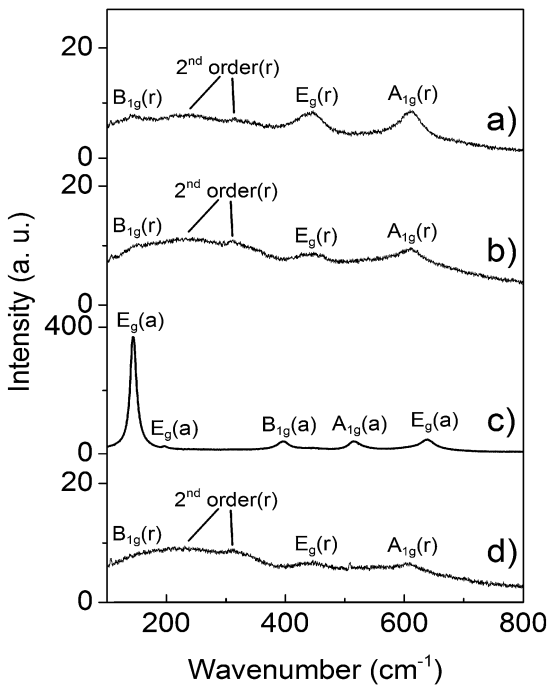

Fig. 3 Raman spectra of Ti foil after thermal annealing, native (a), passivated in HNO_3 (b), etched 1 h in H_2O_2 at 95 °C (c), or etched 48 h in H_2O_2 at room temperature (d). (c) and (d) were both performed after passivation in HNO_3. The vibrational modes of either rutile (r) or anatase (a) were assigned according to ref. 13–15.

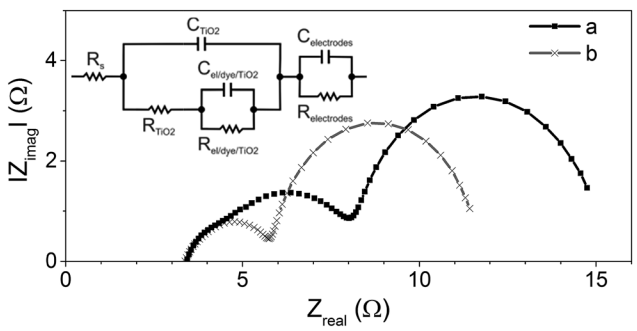

Fig. 4 Nyquist plots of DSSCs with Ti foil as working electrode substrate which was native (a) and passivated in HNO_3 (b). EIS data were obtained at V_{OC} and 100 mW cm^{-2} simulated AM 1.5 sunlight illumination in a frequency range from 0.3 MHz to 2 Hz. The equivalent circuit diagram used for fitting the data is displayed in the inset.

Table 2 Resistances (R) and energy conversion efficiencies (η) of back-illuminated DSSCs with differently treated titanium foils as the working electrode substrate. Estimated errors for each EIS parameter as given by the fitting algorithm are given in brackets

Treatment	R_S (Ω)	R_{TiO_2} (Ω)	$R_{el/dye/TiO_2}$ (Ω)	$R_{electrodes}$ (Ω)	η (%)
Native	3.6 (0.8%)	3.0 (2.2%)	6.7 (2.0%)	1.5 (4.0%)	4.8
HNO_3	3.5 (0.5%)	1.4 (3.6%)	5.6 (1.0%)	1.0 (5.5%)	5.6

is in parallel with the resistance R_{TiO_2} of this nanoporous network and the $RC_{el/dye/TiO_2}$ element which represents the charge-transfer at the electrolyte/dye/TiO_2 interfaces in the pores. The $RC_{electrodes}$ element includes the charge-transfer resistances at the counter electrode or rather electrolyte/Pt/FTO interface and at the TiO_2/Ti interface of the working electrode.

As expected, the passivation of Ti foils with nitric acid does not significantly influence R_S. However, the resistance at the titanium/TiO_2 interface decreases as $R_{electrodes}$ decreases while there are no changes on the counter electrode. This may be a consequence of the removal of surface impurities.

R_{TiO_2}, the resistance between TiO_2 particles (as well as the passivation layer), is halved, which indicates a significant enhancement of the electron transport within the TiO_2 film of the photoanode. This may be due to better attachment of the TiO_2 nanoparticles on the improved passivation layer of the foil, providing better electrical contact to the electrode substrate. Additionally, lower (16%) resistance at the electrolyte/dye/TiO_2 interface after passivation in nitric acid (also in regard of the increased V_{OC}), suggests, that improved homogeneity of the passivated film suppresses electron leakage at the Ti substrate/TiO_2/electrolyte interface.

As has been shown before for stainless steel, reduction in electrical resistance at the TiO_2/conductive layer interface, achieved electrochemically using sulphuric acid, enhances both J_{SC} and η, however V_{OC} and FF remained nearly constant in this case.[21]

Other groups reported the improved efficiency of back-illuminated DSSCs with TiO_2 interlayers on Ti foils is also caused by an enhancement of the reflectance properties of the foil surface directing light back into the TiO_2-dye film on the anode.[4,5]

In Fig. 5, reflectance and IPCE transients for native and passivated foils are shown. In the wavelength range from *ca.* 400 to 600 nm the reflectance of the foil with passivation layer is slightly lower and for higher wavelengths it is marginally higher. However, the IPCE curve of the DSSC assembled with HNO_3 passivated Ti foil shows higher values over nearly the whole dye-absorbing wavelength range. Therefore, it is concluded that reflectance properties do not play a role for the efficiency improvement through the rutile passivation interlayer in our case.

The stability of DSSCs is very important and so we have looked at the effect of the foil treatments on the photovoltaic performance of the DSSCs over time. After initial characterization, the solar cell devices were stored under atmospheric conditions in the dark and tested again after 20 days. The results of these J–V measurements are listed in Table 1. While

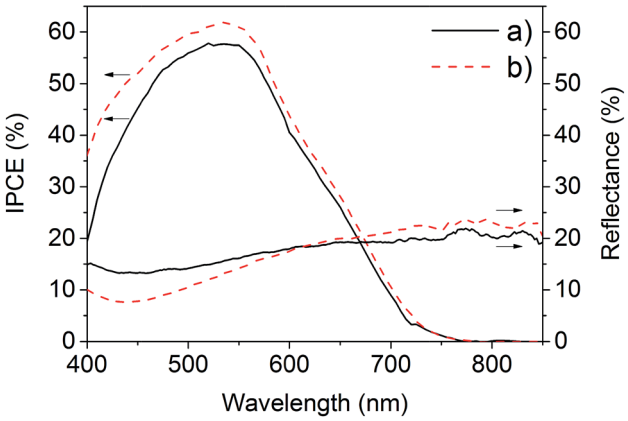

Fig. 5 Incident photon to current efficiency (IPCE) of DSSCs and reflectance of working electrode substrates of native (a), and in HNO_3 passivated (b), Ti foils.

the conversion efficiencies of the DSSCs with non-treated and H_2O_2-etched Ti foils decrease significantly, the solar cells with HNO_3 passivated foils lose just 0.1% η, which is within the error range of the value determined right after assembling. The highest degradation is shown by the devices assembled with the native Ti foil whose efficiency decreased from 4.8% to 1.8%.

The passivation layers on the foil likely prevent the loss of solar cell performance by ensuring a stable and uniform surface layer onto which the TiO_2 nanoparticle layer is attached. In contrast, the H_2O_2 treatments, are not only less effective but actually reduce the beneficial effect of the HNO_3 passivation layer, especially in the case of the high-reaction rate conditions at 95 °C (Table 1). This is seen through changes in V_{OC} and FF, but most significantly through consistent decreases in J_{SC}, implying an increase in anode resistance. Therefore, it is suggested that the dense passivation layer produced by the HNO_3 treatment (Fig. 1b) is profoundly affected during the H_2O_2 treatments while the thicker porous layers introduced through these treatments do not enhance the properties of the DSSCs.

We also fabricated DSSCs with HNO_3 passivated Ti foil as the working electrode substrate where we dipped the screen-printed and annealed photoelectrodes into an aqueous 0.02 M $TiCl_4$ solution for 30 min at 70 °C. The resulting solar cell devices have a further increased efficiency of 6.1 ± 0.2% (J_{SC} = 10.74 mA cm^{-2}, V_{OC} = 770 mV, FF = 0.73). This demonstrates that the performance of the back-illuminated DSSCs investigated in this study can be further enhanced by optimizing other device parameters, which were not examined here.

Conclusions

A simple HNO_3 passivation treatment enhanced the properties of the thin, native rutile layer on Ti foils. Using these foils as photoanode substrates in back-illuminated DSSCs improved the photovoltaic performance of the devices due to enhanced electron transport in the TiO_2 film. Furthermore, the stability of the solar cells was significantly prolonged.

Acknowledgements

The authors acknowledge use of the facilities and the assistance of Tony Romeo at the UOW Electron Microscopy Centre and Patricia Hayes in the Australian National Fabrication Facility (ANFF). This research was carried out with the support of the Australian Cooperative Research Centre for Polymers, ANFF and the German National Academic Foundation (scholarship for JL).

Notes and references

1 K. Fan, T. Peng, B. Chai, J. Chen and K. Dai, *Electrochim. Acta*, 2010, **55**, 5239–5244.
2 K. Onoda, S. Ngamsinlapasathian, T. Fujieda and S. Yoshikawa, *Sol. Energy Mater. Sol. Cells*, 2007, **91**, 1176–1181.
3 C.-H. Lee, W.-H. Chiu, K.-M. Lee, W.-F. Hsieh and J.-M. Wu, *J. Mater. Chem.*, 2011, **21**, 5114–5119.
4 J. An, W. Guo and T. Ma, *Small*, 2012, **8**, 3427–3431.
5 C.-H. Lee, P.-T. Hsiao, M.-D. Lu and J.-M. Wu, *RSC Adv.*, 2013, **3**, 2216–2218.
6 C. Y. Hsu, S. J. Cherng, Y. J. Lin and C. M. Chen, *IEEE Electron Device Lett.*, 2013, **34**, 1415–1417.
7 T. Y. Tsai, C. M. Chen, S. J. Cherng and S. Y. Suen, *Prog. Photovoltaics*, 2013, **21**, 226–231.
8 R.-H. Tao, J.-M. Wu, H.-X. Xue, X.-M. Song, X. Pan, X.-Q. Fang, X.-D. Fang and S.-Y. Dai, *J. Power Sources*, 2010, **195**, 2989–2995.
9 E. Gee, L. Golden and W. Lusby, *Ind. Eng. Chem. Res.*, 1949, **41**, 1668–1673.
10 C. Sitting, M. Textor and N. D. Spencer, *J. Mater. Sci.: Mater. Med.*, 1999, **10**, 35–46.
11 J. Been and D. Tromans, *Corrosion*, 2000, **56**, 809–818.
12 J.-M. Wu, S. Hayakawa, K. Tsuru and A. Osaka, *Scr. Mater.*, 2002, **46**, 101–106.
13 T. Ohsaka, *J. Phys. Soc. Jpn.*, 1980, **48**, 1661–1668.
14 V. Swamy, B. C. Muddle and Q. Dai, *Appl. Phys. Lett.*, 2006, **89**, 163118.
15 H. C. Choi, Y. M. Jung and S. B. Kim, *Vib. Spectrosc.*, 2005, **37**, 33–38.
16 T. Hoshikawa, M. Yamada, R. Kikuchi and K. Eguchi, *J. Electrochem. Soc.*, 2005, **152**, E68–E73.
17 R. Kern, R. Sastrawan, J. Ferber, R. Stangl and J. Luther, *Electrochim. Acta*, 2002, **47**, 4213–4225.
18 Q. Wang, S. Ito, M. Grätzel, F. Fabregat-Santiago, I. Mora-Seró, J. Bisquert, T. Bessho and H. Imai, *J. Phys. Chem. B*, 2006, **110**, 25210–25221.
19 R. Li, D. Liu, D. Zhou, Y. Shi, Y. Wang and P. Wang, *Energy Environ. Sci.*, 2010, **3**, 1765–1772.
20 K. Wagner, M. J. Griffith, M. James, A. J. Mozer, P. Wagner, G. Triani, D. L. Officer and G. G. Wallace, *J. Phys. Chem. C*, 2011, **115**, 317–326.
21 H. G. Yun, Y. Jun, J. Kim, B. S. Bae and M. G. Kang, *Appl. Phys. Lett.*, 2008, **93**, 133311.

